공학석사학위논문

Thermo-elastic analysis of structurally damped functionally graded plate with micro-mechanical properties

미시기계적 물성을 가진 구조감쇠 경사기능재료의 열-탄성 해석

2016 년 2월

서울대학교 대학원

기계항공공학부

이 영 훈

Abstract

Thermal post-buckling and limit-cycle oscillation characteristics of structurally damped functionally graded materials (FGMs) plate are studied based on neutral surface using homogenization method. Especially, the materials have non-homogeneous properties with varying gradually from one surface to the other. Material properties are assumed to be temperature dependent and neutral surface is adopted reference plane due to of asymmetry of the material properties in the thickness direction, because the mid-plane of the FGMs plate model is not equal to the neutral surface of the structure. Homogenization modeling of FGMs plates are investigated in the thermo-mechanical environment, and it is more actual method to approach FGMs analysis. In this regard, Mori-Tanaka Scheme (MTS) explicitly evaluates particle interactions, and the governing formulation is based in first-order shear theory (FSDT) and the von Karman strain-displacement equation to consider geometric nonlinearity. Newton-raphson method is applied solve the thermal post-buckling analysis, and time integration is applied to solve the limit-cycle oscillation by using Newmark's method. In order to validate the post-buckling and limit-cycle oscillations, results are compared with previous data of continuous FGMs model. The influence of homogenized model and neutral surface on the thermo-mechanic analysis of FGMs is also highlighted.

Key words : Functionally graded materials, Thermal post-buckling, Limit-cycle oscillation, Neutral surface, Mori-Tanaka scheme

Student Number : 2014-20679

Contents

Abstract ····· **i**

Contents ····· **ii**

List of Tables and Figures ····· **iii**

List of Nomenclature ····· **iv**

1. Introduction ····· **1**

2. Formulation ····· **4**

2.1 Functionally graded materials ····· **4**

2.2 Physical neutral surface ····· **5**

2.3 Homogenization scheme ····· **5**

3. Governing equation ····· **8**

3.1 Temperature rise ····· **8**

3.2 Constitutive equation ····· **9**

3.3 Method of analysis ····· **11**

3.4 Static and dynamic problem ····· **12**

3.4.1 Static analysis ····· **13**

3.4.2 Dynamic analysis ····· **13**

4. Numerical Results and Discussion ····· **14**

4.1 Code verification ····· **14**

4.2 Thermal post-buckling behavior ····· **15**

4.2.1 Temperature-dependent problem ····· **16**

4.2.2 Heat transfer effect ····· **17**

4.3 Thermal limit-cycle oscillation ····· **18**

5. Conclusions and Future works ····· **20**

References ····· **21**

국문 초록 ····· **48**

List of Table and Figure

Tables

Table 1. Temperature-dependent material properties of metal and ceramic

Table 2. Flutter boundaries of FGMs with and without structurally damping.

Table 3. Comparison of up and down-side deflection according to reference plane

Table 4. Comparison of up and down-side deflection using homogenized properties.

Table 5. Limit cycle amplitudes according to reference plane.

Table 6. Limit cycle amplitudes using homogenized properties.

Figures

Fig. 1. A FGM plate model.

Fig. 2. Effective materials properties through the thickness distribution.

(a) Young′s modulus ; (b) Poisson′s ratio

Fig. 3. Non-dimensional neutral surface position from mid-plane.

Fig. 4. Comparison of the effective properties

(a) Variation of Young's modulus; (b) Poisson's ratio

Fig. 5. Non-dimensional center deflections for boundary conditions

Fig. 6. Linear thermal buckling temperature based on neutral surface

(a)Thickness; (b) Aspect ratio

Fig. 7. Center deflection with and without damping effect ($T = 300K + \Delta T$)

(a) Simply-supported boundary condition; (b) Clamped

Fig. 8. Neutral surface shift due to volume index and temperature.

Fig. 9. Center deflection according to reference plane

($T = 300K + \Delta T$)

(a) Simply-supported boundary condition; (b) Clamped

Fig. 10. Homogenized modulus of FGMs plate

(a) Bulk modulus ; (b) Shear modulus

Fig. 11. Center deflection according to homogenized properties

($T = 300K + \Delta T$)

(a) Simply-supported boundary condition; (b) Clamped

Fig. 12. Center deflection with and without damping effect

considering heat conduction ($T = 300K + \Delta T$)

(a) Simply-supported boundary condition; (b) Clamped

Fig. 13. Center deflection according to reference plane considering heat conduction

($T = 300K + \Delta T$)

(a) Simply-supported boundary condition; (b) Clamped

Fig. 14. Center deflection according to homogenized properties considering

heat conduction ($T = 300K + \Delta T$)

(a) Simply-supported boundary condition; (b) Clamped

Fig. 15. LCO of plates according to reference plane without heat transfer effect

(a) Simply-supported boundary condition; (b) Clamped

Fig. 16. LCO of plates according to reference plane with heat transfer effect

(a) Simply-supported boundary condition; (b) Clamped

Fig. 17. LCO of plates using homogenized properties with heat transfer effect

(a) Simply-supported boundary condition; (b) Clamped

List of Nomenclature

A	In-plane stiffness matrix
A_d	Aerodynamic damping matrix
A_f	Aerodynamic influence matrix
A_s	Transverse shear stiffness
a	Plate length
B	In-plane bending coupling stiffness matrix
$B(z,T)$	Bulk modulus
b	Plate width
C_R	Reduced damping matrix
D	Bending stiffness matrix
d	Displacement vector
E	Young's modulus
f	External force vector
$G(z,T)$	Shear modulus
h	Plate thickness
K	Linear elastic stiffness matrix
$K(z,T)$	Heat conductivity
$K_{\Delta T}$	Thermal stiffness matrix
K_R	Reduced stiffness matrix
k	Volume fraction index
k_p	Shear correction factor
M	Mass matrix
$M_b, M_{\Delta T}$	Moment resultant and thermal moment resultant, respectively
M_R	Reduced mass matrix
$N_b, N_{\Delta T}$	In-plane force resultant and thermal in-plane force resultant, respectively
$N1, N2$	First-order non-linear stiffness and second-order non-linear stiffness matrices, respectively
P, P_{eff}	Material property and effective material property
$P_{\Delta T}{}^*$	Thermal load vector

Q_s	Transverse shear force resultant vector
$T,$	Temperature
T_i, T_f	Reference temperature and final temperature, respectively
ΔT	Temperature elevation
u	In-plane displacement in the x direction
v	In-plane displacement in the y direction
V	Volume fraction
w	Transverse displacement in the z direction
z_0	Neutral surface shift
$\partial W_{\text{int}}, \partial W_{ext}$	Internal and external virtual
α	Thermal expansion coefficient
λ	Non-dimensional aerodynamic pressure
ϕ_x, ϕ_y	Rotation of the normal in the xz and yz plane, respectively
φ_0	Time independent vector
ω	Plate motion parameter
ρ	density of ring material
σ	stress

Subscripts

cr	Critical
c	Ceramic
m	Metal
s	Static state
t	Dynamic state

1. Introduction

Composite material is defined as a combination of two or more distinct materials to create a new material with properties. It can be determined that a wide range of engineering situation. Functionally graded materials (FGMs) is a representative composite materials to use various environments. The concept of FGMs was originated in mid-1980 in Japan during a space plane project in which a combination of materials was used to act as thermal barrier. [1] Since the material compositions of FGMs are varied gradually from a materials to another one, those interface problems can be effectively reduced. [2]

FGMs have been emerged from manufacturing a composite material in high temperature status. Specifically, FGMs are made of the continuous mixture of ceramic and metal and then the material properties smooth and continuous pattern from one surface to the other as compared with conventional composite, and ceramic has high compressive strength and heat resistance with low fracture toughness, but metal exhibits better mechanical strength while cannot withstand at high thermal environment. These attractive merits have increased the roles of FGMs in various engineering fields. In particular, FGMs plate made of a ceramic and a metal can be used as an outer wall of a space model which is subjected to high temperature changes. In this case, when the model flies under high thermal environments, the plates can be experience serious structural problems, such as thermal buckling or flutter. Therefore, it is necessary to study the thermal post-buckling and flutter analysis of FGMs plates to ensure reliable design.

For about three decades, numerous research works of thermal buckling and post-buckling on the materials have been performed. Bouazza et al.[3] studied the thermo-elastic buckling behavior of structures based on First-order Shear Deformation Theory (FSDT). Further, Bouiadjra et al.[4] analyzed the thermal buckling behavior of the model using a refined plate theory. Further, S. R. Li et al. [5] presented analysis of thermal post-buckling of FGMs Timoshenko beams subjected to transversely non-uniform temperature rise. Prakash et al. [6] investigated the post-buckling behavior of FGM skew plate under thermal load based on shear deformable finite element approach. Shen [7] reported thermal post-buckling analysis for a simply supported, shear deformable FGMs plate under thermal loading. Lee and Kim [8] studied the supersonic aero-thermo post-buckling behaviors and limit-cycle oscillations of FGM panels using Newmark's time integration method. Lee and Kim [9] performed the thermo-mechanical behavior of FGM panels in hypersonic airflows. Achchhe Lal et al. [10] examined the second-order statistics of post-buckling of FGM subjected to mechanical and thermal loading with non-uniform temperature changes subjected to temperature independent and

dependent material properties. Liew et al. [11] presented thermal buckling and post-buckling analysis for moderately thick laminated rectangular plates that contain FGMs and subjected to a uniform temperature change.

Recently, as the use of FGMs plates for space models is expected to increase, researches on dynamic characteristics and stability of FGMs plate are being performed. Navazi and Haddapour [12] determined the aero-thermoelastic stability margins of FGM plates using analytical approach. Sohn and Kim [13] investigated static and dynamic stabilities of FGM panels which are subjected to combines thermal and aerodynamic loads. Prakash and Ganapathi [14] investigated the influence of thermal environment on the supersonic flutter behavior of flat plates made of functionally graded materials using finite element procedure. Lee et al. [15] performed flutter analysis of stiffened laminated plates to analyze the dynamic characteristics of stiffened plates subjected to thermal load. Ibrahim et al. [16] studied the non-linear flutter and thermal buckling of FGM panels under the combined effect of elevated temperature conditions and aerodynamic loading. Haddapour et al. [17] revealed the nonlinear aeroelastic behavior of FGM plates in supersonic flow.

For equilibrium of structure, neutral surface has been used as a reference plane due to the asymmetry of material properties in the thickness direction of FGMs as compared with the previous works. Prakash and Singha [18] studied nonlinear behavior of FGMs skew plates under in-plane load. Zhang [19] considered a higher-order shear deformation theory of the plate models for thermal buckling behavior using the neutral concept. Yaghoobi and Fereidoon [20] indicated the influence of neutral surface position on deflection.

However, these research works considered only in the macroscopic material properties of FGMs, and more reliable data for the structure can be obtained using micromechanical level estimation of the properties. Mori and Tanaka [21] originally concerned with an estimation of the average internal stress in matrix of a material containing precipitates with eigen-strains for composite materials. Therefore, numerous analysis of homogenized FGMs are studied in various environments. Shen and Wang [22] considered the small and large amplitude vibration for a FGMs plates resting in a two-parameter elastic foundation in thermal environments. Kiani and Eslami [23] investigated thermal post-buckling of solid circular plates made of a through-the-thickness FGMs on three different homogenization schemes. Akabarzadeh et al. [24] examined the influence of alternative micro-mechanical models on the macroscopic behavior of a FGMs plate based on classical and shear-deformation plate theories.

In this paper, thermal post-buckling and limit-cycle oscillation characteristics of FGMs plate are studied based on neutral surface using homogenization method. The plates are considered as

temperature dependent model in thermal environments, and models are assumed as plates based on the first-order shear deformation theory. Material properties of the plates with temperature dependent are continuously varied in the thickness direction, and adopted micro-mechanical characteristic. For the microscopic modeling of the structure, Mori-Tanaka Scheme (MTS) is employed for more accurate estimation of material properties. Also, aim of present study is to use the neutral surface concept, and the results compares the post-buckling and limit-cycle oscillation characteristics with the previous data based on conventional reference plane. In order to discuss the present works, the cases of models are considered with and without heat conduction effects in the thickness direction.

2. Formulation

FGMs with temperature dependent material properties are presented with length a, width b and thickness h. In this work, the formulation is based on the first-order shear deformation theory of plate with and without considering heat transfer effects.

2.1. Functionally graded materials

A mixture of ceramic and metal is studied of the model, and the mixture ratio is varying continuously and smoothly in the thickness direction.

Thus, the volume fraction of the material is defined as simple power-law:

$$V_c(z) = \left(\frac{z}{h} + \frac{1}{2}\right)^k \quad (0 \le k < \infty), \qquad V_c(z) + V_m(z) = 1 \tag{1}$$

where V_c, superscript k, subscripts c and m, superscript h represent the volume fraction of ceramic, the volume fraction index, ceramic and metal, thickness of plate model, respectively.

Generally, the temperature dependent material properties $P(T)$ are written as in Ref. [25].

$$P(T) = P_0\left(\frac{P_{-1}}{T} + 1 + P_1 T + P_2 T^2 + P_3 T^3\right) \tag{2}$$

where T stands for the temperature, and P_0, P_{-1}, P_1, P_2 and P_3 are constants in the cubic fit of the material properties. While, using the rule of mixture (ROM):

$$\begin{aligned} P_{\text{eff}}(z,T) &= P_m(T)V_m(z) + P_c(T)V_c(z) \\ &= P_m(T) + (P_c(T) - P_m(T))\left(\frac{z}{h} + \frac{1}{2}\right)^k \end{aligned} \tag{3}$$

where subscript *eff* means effective of all the properties, such as Young's modulus, thermal expansion coefficient, thermal conductivity and Poisson's ratio, respectively.

2.2. Physical neutral surface

Fig. 1 shows FGMs model with the middle and the neutral surfaces, and precisely the material properties in the thickness direction are asymmetric. In this study, the neutral surface is chosen as a reference plane for deformation, based on the force equilibrium of the model.

Including the thermal effect on the FGMs plate, integration in the thickness direction for the first moment of elasticity modulus $E(z,T)$ equals to zero to determine the neutral surface of the model.

$$\int_{-\frac{h}{2}}^{\frac{h}{2}} E(z,T)(z-z_0(T))dz = 0 \tag{4}$$

Thus, the position of neutral surface $z_0(T)$ can be obtained as [26]

$$z_0(T) = \frac{\int_{-\frac{h}{2}}^{\frac{h}{2}} E(z,T)zdz}{\int_{-\frac{h}{2}}^{\frac{h}{2}} E(z,T)dz} \tag{5}$$

The non-dimensional neutral surface location of FGMs are obtained as :

$$\frac{z_0(T)}{h} = \frac{k(E_c(T)-E_m(T))}{2(k+2)(kE_m(T)+E_c(T))} \tag{6}$$

2.3. Homogenization scheme

Mori and Tanaka [21] originally concerned with an estimation of the average internal stress in matrix of a material containing precipitates with eigen-strains for composite materials. In this regard, the present work reconsiders the application of the Mori-Tanaka Scheme (MTS) to the calculation of effective properties of material. While, the previous method is easy to use, but it does not account for the interaction among adjacent inclusions and also evaluate approximate values of the effective elastic modulus. To consider these interactions, simple relations to find the bulk modulus and the shear modulus of the equivalent homogenized medium are used. Bulk

modulus is defined as the ratio of the infinitesimal pressure increase to the resulting relative decrease of the volume. The locally effective bulk modulus $B(z,T)$ and shear modulus $G(z,T)$ of the temperature-dependent FGMs can be obtained as in Ref. [6].

$$\frac{B(z,T)-B_m(T)}{B_c(T)-B_m(T)}=\frac{V_c(z)}{1+[1-V_c(z)][3B_c(T)-3B_m(T)]/[3B_m(T)+4G_m(T)]} \tag{7}$$

$$\frac{G(z,T)-G_m(T)}{G_c(T)-G_m(T)}=\frac{V_c(z)}{1+[1-V_c(z)][G_c(T)-G_m(T)]/[G_m(T)+f_1(T)]} \tag{8}$$

In Eq. (5), $f_1(T)$ is defined as follows

$$f_1(T)=\frac{G_m(T)[9B_m(T)+8G_m(T)]}{6[B_m(T)+2G_m(T)]} \tag{9}$$

Using Eqns (4)-(5) with (6),Young's modulus, Poisson's ratio, heat conductivity and thermal expansion can be obtained.

For Young's modulus E is given by [22]

$$E(z,T)=\frac{9B(z,T)G(z,T)}{3B(z,T)+G(z,T)} \tag{10}$$

Poisson's ratio ν is expressed as [22]

$$\nu(z,T)=\frac{3B(z,T)-2G(z,T)}{2(3B(z,T)+G(z,T))} \tag{11}$$

The coefficient of thermal expansion α is determined from the relation [27]

$$\frac{\alpha(z,T)-\alpha_c(T)}{\alpha_m(T)-\alpha_c(T)}=\frac{1/K(z,T)-1/K_c(T)}{1/K_m(T)-1/K_c(T)} \tag{12}$$

Further, the effective heat conductivity $K(z,T)$ is given by [28]

$$\frac{K(z,T)-K_m(T)}{K_c(T)-K_m(T)}=\frac{V_c(z)}{1+[1-V_c(z)][K_c(T)-K_m(T)]/3K_m(T)} \tag{13}$$

3. Governing equations

3.1. Temperature rise

Consider a FGMs plate at reference temperature T_i, the uniform temperature is raised in the whole region to T_f without heat conduction, then the structure buckles due to the thermal effect. In this case, the temperature field can expressed as [29]

$$\Delta T = T_f - T_i \tag{14}$$

On the other hand, heat conduction is involved with the coefficient of thermal conduction $K(z)$ depending on thickness z . The property of the conductivity written in terms of z using a power form :

$$K(z,T) = K_m + (K_c - K_m)\left[(2z+h)/2h\right]^k \tag{15}$$

Then, steady-state heat conduction equation and the boundary conditions at the upper and lower surfaces are

$$\frac{d}{dz}\left[K(z,T)\frac{dT}{dz}\right] = 0 \tag{16}$$

with $T = T_c$ at $z = h/2$ and $T = T_m$ at $z = -h/2$.

Thus, the solution for temperature distribution across the plate thickness becomes [19]

$$T = T_c - (T_c - T_m)\frac{\int_{-h/2}^{z}(1/K(z,T))dz}{\int_{-h/2}^{h/2}(1/K(z,T))dz} \tag{17}$$

An interesting thing is that the formula stands for uniform temperature case for $T_c = T_m$.

3.2. Constitutive equations

Introducing the physical neutral surface at $z = z_0(T)$, and assuming the displace fields as [30]

$$\begin{aligned} u(x,y,z,T) &= u_0(x,y) + (z - z_0(T))\phi_x(x,y) \\ v(x,y,z,T) &= v_0(x,y) + (z - z_0(T))\phi_y(x,y) \\ w(x,y,z,T) &= w_0(x,y) \end{aligned} \tag{18}$$

where u, v and w are the displacements in the x, y and z direction, while ϕ_x and ϕ_y are the rotations of the normal in the xz and yz planes, respectively.

The constitutive equations can be obtained defined as

$$\begin{Bmatrix} N_b(T) \\ M_b(T) \end{Bmatrix} = \begin{bmatrix} A & B(T) \\ B(T) & D(T) \end{bmatrix} \begin{Bmatrix} \varepsilon_0 \\ \kappa \end{Bmatrix} - \begin{Bmatrix} N_{\Delta T} \\ M_{\Delta T} \end{Bmatrix}$$

$$[Q_s(T)] = [A_s(T)]\gamma \tag{19}$$

where $[A_s(T)] = k_p \int_{-h/2}^{h/2} \frac{E(z,T)}{2(1+\nu(T))} \begin{bmatrix} 1 & 0 \\ 0 & 1 \end{bmatrix}$

where $N_b(T)$, $M_b(T)$ and $Q_s(T)$ and $A_s(T)$ denote the in-plane force resultant, the moment resultant , the transverse shear force resultant vectors and transverse shear stiffness, respectively.

$$
\begin{aligned}
N_b(T) &= \begin{Bmatrix} N_{xx}(T) \\ N_{yy}(T) \\ N_{xy}(T) \end{Bmatrix} = \int_{-h/2}^{h/2} \begin{Bmatrix} \sigma_{xx}(T) \\ \sigma_{yy}(T) \\ \sigma_{zz}(T) \end{Bmatrix} dz \\
M_b(T) &= \begin{Bmatrix} M_{xx}(T) \\ M_{yy}(T) \\ M_{xy}(T) \end{Bmatrix} = \int_{-h/2}^{h/2} (z - z_0(T)) \begin{Bmatrix} \sigma_{xx}(T) \\ \sigma_{yy}(T) \\ \sigma_{zz}(T) \end{Bmatrix} dz \\
Q_s(T) &= \begin{Bmatrix} Q_y(T) \\ Q_x(T) \end{Bmatrix} = \int_{-h/2}^{h/2} \begin{Bmatrix} \sigma_{yz}(T) \\ \sigma_{xz}(T) \end{Bmatrix} dz
\end{aligned}
\tag{20}
$$

While, A , $B(T)$, $D(T)$ are the in-plane, in-plane bending coupling stiffness and bending stiffness:

$$
(A, B(T), D(T)) = \int_{-h/2}^{h/2} [E](1, (z - z_0(T)), (z - z_0(T))^2) dz \tag{21}
$$

Further, $N_{\Delta T}(T)$ and $M_{\Delta T}(T)$ are the thermal in-plane force resultant and the thermal moment resultant vectors as

$$
\begin{aligned}
\left(N_{\Delta T}(T), M_{\Delta T}(T)\right) &= \begin{pmatrix} N_{\Delta Tx} & M_{\Delta Tx} \\ N_{\Delta Ty} & M_{\Delta Ty} \\ N_{\Delta Txy} & M_{\Delta Txy} \end{pmatrix} \\
&= \int_{-h/2}^{h/2} (1, (z - z_0(T)))[E] \begin{pmatrix} \alpha(z,T) \\ \alpha(z,T) \\ 0 \end{pmatrix} \Delta T(z) dz
\end{aligned}
\tag{22}
$$

where, the temperature dependent elastic coefficient matrix is

$$[E]=\frac{E(z,T)}{1-v^2}\begin{bmatrix}1 & v & 0\\ v & 1 & 0\\ 0 & 0 & \dfrac{1-v}{2}\end{bmatrix} \tag{23}$$

Further, ε_0 and κ are strain vectors based on midpoint and curvature. k_p denote the transverse shear correction coefficient as Ref. [31].

$$k_p=\frac{5}{6-(v_cV_c+v_mV_m)} \tag{24}$$

where v_c and v_m denote the Poisson's ratio of ceramic and metal, respectively.

3.3. Method of analysis

The principle of virtual work is used to derive the equations of motion

$$\delta W=\delta W_{\text{int}}-\delta W_{ext}=0 \tag{25}$$

where ∂W_{int} and ∂W_{ext} represent the internal virtual work and the external virtual work, respectively.

$$\begin{aligned}\delta W_{\text{int}}&=\int_V \delta e^T dV=\int_A[\delta\varepsilon^T N+\delta\kappa^T M+\delta\gamma^T Q]dA\\ &=\delta d^T[K^e-K_{\Delta T}+\frac{1}{2}N1+\frac{1}{3}N2]d-\delta d^T P_{\Delta T}\end{aligned} \tag{26}$$

In Eq. (26), $d=[u,v,w,\phi_x,\phi_y]^T$ is the displacement vector. In addition, K^e is the global bending stiffness matrix obtained by assembling the A, $B(T)$, $D(T)$ matrix and K^T is the

global thermal stiffness matrix in terms of $N_{\Delta T}(T)$. Also, $N1, N2$ and $P_{\Delta T}$ are matrices that denotes the first-order non-linear stiffness, the second-order non-linear stiffness and thermal load vector, respectively.

$$\delta W_{ext} = \delta d^T f = \int_A (P_{air}) \delta w dA = -\delta d^T \{\lambda dA_f + A_d\, d\} \tag{27}$$

Finally, the discredited form of the governing equations of the FGMs plates is obtained as:

$$M\, d + (\alpha_0 M + \alpha_1 K + \frac{g_a}{\omega_0} A_d)\, d + (K - K_{\Delta T} + \lambda A_f + \frac{1}{2} N1 + \frac{1}{3} N2) d = P_{\Delta T} \tag{28}$$

where the coefficient matrix of d represents all the damping effects, the first two terms capture the structural-damping effect and the remaining terms stand for the aerodynamic-damping coefficients [32].

3.4. Solutions of nonlinear method of analysis

The solution of Eq. (28) is assumed as $d = d_s + \Delta d_t$, where d_s and d_t represent the time independent and time dependent solutions, respectively.

Then, two set of coupled governing equations are obtained as:

$$(K - K_{\Delta T} + \lambda A_f + \frac{1}{2} N1_S + \frac{1}{3} N2_S) d_s = P_{\Delta T} \tag{29}$$

and

$$\begin{aligned} &M\, d_t + (\alpha_0 M + \alpha_1 K + \frac{g_a}{\omega_0} A_d)\, d_t \\ &+ (K - K_{\Delta T} + \lambda A_f + \frac{1}{2} N1_s + \frac{1}{3} N2_s + N2_{st} + \frac{1}{2} N1_t + \frac{1}{3} N2_t) d_t = 0 \end{aligned} \tag{30}$$

where the subscript s and t, represent the static and dynamic states, respectively. Eq. (29) is the equation of motion for static analysis such as a thermal post-buckling analysis. On the other

hand, Eq. (30) is the equation of motion for dynamic problem like the vibration or flutter behaviors, and then the static equation should be solved before due to they are coupled.

3.4.1 Static analysis

In this section, a solution procedure for thermal post-buckling analysis is presented. To analyze the thermal post-buckling behavior of the FGMs plates, the incremental form of Eq. (29) is obtained by using the Newton-Raphson iterative method as in Ref. [15].

$$(K - K_{\Delta T} + \lambda A_f + \frac{1}{2} N1_S + \frac{1}{3} N2_S)_i \Delta d_{si+1} = \Delta f_i \tag{31}$$

where the incremental force vector and the updated displacement vector expressed as

$$\Delta f_f = P_{\Delta T} - (K - K_{\Delta T} + \lambda A_f + \frac{1}{2} N1_s + \frac{1}{3} N2_s)_i d_{si}$$

and

$$d_{si+1} = d_{si} + \Delta d_{si+1}$$

The post-buckling behaviors are calculated repeat until to converged incremental displacement.

3.4.2 Dynamic analysis

The dynamic analysis is employed to obtain the critical conditions for the flutter motion of the model. Assuming a increment in the time dependent solution, Δd_t, the time dependent non-linear stiffness matrices, $N1_t$, $N2_t$ and $N2_{st}$ become zero. Thus equilibrium equation is expressed as:

$$M \Delta d_t + (\alpha_0 M + \alpha_1 K + \frac{g_a}{\omega_0} A_d) \Delta d_t + (K - K_{\Delta T} + \lambda A_f + N1_s + N2_s) \Delta d_t = 0 \tag{32}$$

The solution of Eq.(32) is assumed $\Delta d_t = \varphi_0 e^{\omega t}$ and the degrees of freedom can be reduced by Guyan reduction [33]. Further, φ_0 is a time independent vector, and the plate motion parameter ω is a complex number defined as $\omega = \omega_R + i\omega_I$. Then, the reduced homogeneous equations for eigen analysis with state variables can be written as:

$$\left[\begin{bmatrix} 0 & M_R \\ K_R & C_R \end{bmatrix} - \omega \begin{bmatrix} M_R & 0 \\ 0 & -M_R \end{bmatrix}\right] \begin{Bmatrix} \Delta d_t \\ \Delta d_t \end{Bmatrix} = 0 \tag{33}$$

where M_R, K_R and C_R are the reduced mass, stiffness and damping matrices, respectively.

4. Numerical results and discussions

In this section, numerical results of thermal post-buckling and limit-cycle oscillation characteristic of FGMs are performed as $Si_3N_4 / SUS304$. Elasticity modulus, coefficient of thermal expansion and thermal conductivity for constituent materials listed Table 1 as in Ref. [25]. To obtain the numerical results, 7x7 elements with nine-node model is used for each element, and the results for simply-supported and clamped boundary conditions are discussed. Further, the Rayleigh damping coefficient are used for damped model, such as $\alpha = 3.7/s$ and $\beta = 0.762 \times 10^{-2} s$, and a reduced integration [34] method is applied to prevent the transverse shear locking effect.

The contents of this section are summarized as follows : The first section represents the verification with previous data. The second section shows the thermal post-buckling analysis based on neutral surface using MTS. Next, limit cycle oscillations of the models based on previous characteristics in thermal environment are studied in the last section.

4.1. Code verification

For the code verification, results are compared with the previous data. Firstly, the non-dimensional shift(z_0 / h) of neutral surface from the mid-plane is obtained as in Fig. 3 to verify neutral surface shift for the temperature independent materials. Figure shows the volume index along neutral surface, and then the maximum of the neutral surface shift value is 3.8% from mid-plane of FGMs model. The results agree well with the previous work in Ref. [30]. The non-dimensional shift increase with the increase of volume index and reaches maximum value, and the curve drops down asymptotically. As the elasticity modulus difference is increased, the distance between neutral surface and mid-plane is increased.

Then, the maximum value ($k_{\max}(T)$) of $z_0(T)/h$ is obtained as [20]:

$$k_{\max}(T) = \sqrt{2\frac{E_c(T)}{E_m(T)}} \tag{34}$$

Maximum value of the shift $k_{\max}$ is 1.76 and is reasonable with the result in Ref. [30].

Secondly, the materials properties using ROM and MTS are plotted in Fig. 4. The results are compared with the previous and experimental data for Young's modulus and Poisson's ratio of Al/TiC in Ref. [35] for k=1. The evaluated properties in this work using ROM and MTS agree well with the previous work in Ref. [36], and results are quite similar with the experimental data.

Thirdly, the linear thermal buckling is appeared before thermal post-buckling, and then it is necessary to verify linear buckling problem. Thermal buckling temperature of FGMs plate with simply-supported based on neutral surface are verified in Ref. [30], and result using MTS are confirmed as in Ref. [37] shown in Fig.5.

Fourthly, Fig.6 represents thermal post-buckling behavior of FGMs according to reference planes with simply-supported and clamped boundary conditions for $a/h = 1/100$. In the figure, group "A" and "B" confirm correctly with the results as in Ref. [13].

Lastly, to verify the thermal flutter and frequencies for damped FGMs plate, Table. 2 shows the results as compared with the un-damped data as in Ref. [6] and those of damped model as in Ref. [38] for $T_m = T_c$. In the table, subscript cr depict un-damped critical values and dcr express for the results with damping effect considered. Further, the structural damping effects are considered by using the Rayleigh damping coefficients, and the damping influence the flutter speed and lead to the models to be more flexible.

4.2. Thermal post-buckling behavior

In this part, thermal post-buckling behavior of FGMs plate are investigated with and without heat transfer effect, and results are investigated without aerodynamic effect. The temperature is increased continuously by ΔT from $300K$ to $300K + \Delta T$.

4.2.1. Behavior without heat transfer effect

In this section, thermal post-buckling behavior of FGMs plate are investigated without heat transfer effect. The non-dimensional center deflection with and without damping effect of FGMs plate are expressed Fig. 7 for simply supported and clamped boundary condition, respectively. Fig. 7. (a) shows the two equilibrium point for volume fraction $k = 1$, A and B, at $\Delta T = 30K$, and the plate is deformed upward as the temperature decreasing from equilibrium point. As the temperature is decreased, the point B moves to point C, a snap-through could occurred due to the plate want to return to primary equilibrium point, and then the point C jumps to the point D immediately. However, a snap-through and bifurcation are delayed

from the previous model due to the effect of structural damping, and damping extend the value of total difference temperature from equilibrium point B to E. The post-buckling behavior of a simply-supported plates are different from result of clamped condition, and the results for clamped represent bifurcation buckling characteristics of isotropic plates in Fig. 7.(b).

From now on, neutral surface shifts are discussed for Si_3N_4 / $SUS304$ with temperature dependent material properties. Fig. 8 shows the effect of temperature variations according to the position of neutral surface, and interesting thing is that k increases, then the difference of the deviation amount also increased. Therefore, neutral surface are applied in thermal post-buckling analysis due to asymmetric of material property, and the post-buckling results are compared according to reference plane in Fig. 9. As temperature are increased, the center with simply-supported moves to down-side more slowly than the results with mid-plane in Fig. 9 (a). While the previous of snap-through is started at $\Delta T = 16K$, the point are occurred early at $\Delta T = 20K$ from equilibrium point using neutral surface concept. On the other hands, Fig. 9 (b) reveals almost the same results of the deflection for all clamped boundary conditions of models. In this regard, clamped boundary conditions may be more stable than simply-supported edges for thermal post-buckling. Another interesting point is that the difference of up and down side deflection differ between mid-plane and neutral surface as detailed in Table. 3.

Table 3 shows the difference defined as :

$$Difference\ (\%) = \frac{d_s - d_p}{d_p} \times 100\% \tag{35}$$

where d_s and d_p are the deflection after snap-through and previous, respectively.

These buckling deflection of simply-supported plates are due to the asymmetric material properties for mid-plane, and asymmetric stress variation occurs in bending moments. The previous model as mid-plane has jumping point at $\Delta T = 16K$ and difference error about 39% with both side, as the temperature increased, the errors are decreased asymptotically. On the other hands, present model as neutral surface has snap-through point at $\Delta T = 20K$ and the difference about 25.6%, and symmetric deflection of the model is restored at $\Delta T = 80K$ more fast than previous model.

Further, the micro-mechanical properties are adopted in thermal post-buckling analysis in order to consider particle interaction of FGMs. Before analysis, bulk and shear modulus which consist of homogenized material properties are verified in Fig. 10 as compared with the data in Ref. [36]. Fig. 11 compares the deflection with previous and result for homogenized material

properties. As shown Fig. 11 (a), the center position with homogenized properties moves to down-side faster than previous model as temperature increase, and snap-through are delayed at $\Delta T = 14K$ from equilibrium point due to decreasing stiffness term of A, $B(T)$, $D(T)$ matrix. In the Fig. 11 (b), the bifurcation point present at $\Delta T = 36K$ early using Mori-Tanaka scheme for volume fraction $k = 0$, and the point reveal at $\Delta T = 24K$ for $k = 1$. Therefore, thermal buckling trends are changed by homogenizing material properties regardless of boundary conditions. In Table. 4, an interesting things is that the snap-through are delayed at $\Delta T = 14K$ and has more large difference about 59.8%, while the symmetric deflection of the model is restored perfectly at $\Delta T = 60K$ more fast than the model as neutral surface. As a results, homogenized model has best symmetric properties, and then the homogeneous approach for thermal post-buckling are reasonable.

4.2.2. Behavior considering heat transfer effect

Up to now, the heat transfer effects are considered for the analysis in this section, and the temperature of bottom metal part is expressed T_m and the top ceramic part is represented T_c, respectively. The thermal conduction are gradually changed by temperature metal to ceramic for thickness direction. Fig. 12 summarizes the deflection with and without damping effects for two boundary conditions. At low temperature, the plates moves to only up-side direction and has one equilibrium point on up-side stat in Fig. 12 (a). In down-side direction, the snap-through is appeared to jump up-side, and the results are also delayed with damping effect regardless of volume fraction. As shown Fig. 12 (b), the damped model has similar trends with Fig. 7 (b) for clamped boundary condition.

In here, neutral surface of the model is selected as the reference for the thermal post-buckling analysis. Fig. 13 (a) shows the similar trend of deflection with Fig. 12 (a) for simply supported condition, but the jumping point are more delayed than the results without heat transfer effects as in Fig. 9 (a). While the results based on neutral surface without heat conduction has lower value than previous data in Fig. 9 (a), present results with heat conduction has large value than previous work as in Fig. 13 (a). In Fig. 13 (b), the plates has same bifurcation points regardless of reference plane, therefore clamped models are verified for stable condition.

For using homogenized properties, Fig. 14 depicts the result considering heat transfer effects. In Fig. 14 (a), the snap-through point is appeared early than previous model as using rule of mixture method, and the model moves to up-side direction slowly. Further, the bifurcation can

be occurred slowly than the previous model regardless of volume fraction with clamped boundary condition as in Fig. 14 (b). As compare Fig. 11 and Fig. 14, distributions of plate are differ from each condition, and then homogenized heat conduction affects highly than other effective material properties for thermal post-buckling behavior.

4.3. Thermal limit-cycle oscillation with structural damping

FGMs plate has the geometrical non-linearity of structures, and then the thermal limit-cycle oscillations (LCO) can be occurred after critical points. In this part, the LCO with structural damping are studied for various condition, such as boundary condition, reference plane and homogenized material. The volume fraction of FGMs select $k=1$ without aero-dynamic pressure in this dynamic analysis. Fig. 15 represent LCO of the model according to reference plane without heat conduction. As the reference plane is changed, the amplitude of FGMs with simply-supported are increased little as shown in the Fig. 15 (a). The amplitudes of up-side are increased as 0.0693 to 0.0717, and result of down-side are almost same as listed in Table. 5 on without heat conduction section. While, the clamped model has not difference regardless of reference plane in Fig. 15 (b) because the clamped model are more stable than simply-supported model like as thermal post-buckling analysis. And, the detail amplitude of clamped model are always same in Table. 5. As the model consider heat transfer effect, the LCO are changed as shown in Fig. 16. The start point of LCO with heat conduction has opposite from previous model without heat conduction in Fig. 16 (a), and the amplitude of down-side are decreased -0.0739 to -0.0717 as in Table. 5. However, the clamped model with heat conduction has perfectly opposite distribution according to reference plane in Fig. 16 (b).

For considering homogenized properties with heat conduction, the amplitudes of LCO are changed by boundary condition as in Fig. 17. The amplitudes of the model based on MTS are slightly smaller than the results using ROM, and the frequency of LCO increases as shown in Fig. 17 (a) due to the homogenized model affects flexible effect in simply-supported conditions for dynamic analysis. On the other sides, as the boundary condition changes to clamped, the amplitudes based on MTS are slightly bigger than the previous results, and the frequency decreases because of the stiffer effect considering homogenized properties in Fig. 17 (b). In detail, the amplitudes of LCO with two boundary condition are listed in Table 6. In Simply-supported condition, maximum amplitudes are decreased as 0.0717 to 0.0612, and the aspect are opposite in clamped condition. Therefore, results of dynamic analysis based on homogeneous scheme are different according to boundary conditions.

5. Conclusions

In this paper, the influence for neutral surface and homogenized material properties of Functionally Graded Materials (FGMs) plate are studied for the post-buckling and limit-cycle oscillations with the Ray-leigh damping of structural effects in thermal environments. Based on first-order shear deformation theory, the equilibrium and stability equations of functionally graded rectangular plates have been derived. To verify the accuracy of the present theory, the results obtained by the present analysis have been compared with their counterparts in the literature. The neutral surface positions are revealed with various condition such as volume fraction and temperature, and the comparison of the reference plane are investigated using temperature dependent material properties. And then, the homogenized properties of the FGMs plates are calculated using homogeneous scheme such as rule of mixture (ROM) and the Mori-Tanaka Scheme (MTS) based on neutral surface. Furthermore, concept of homogenization scheme is used for advanced results, and the difference of the properties obtained based on ROM and MTS are performed in detail. As shown in static results, the snap-through point are occurred early from equilibrium point using neutral surface concept, and the deflections are almost the same results for all clamped boundary conditions of models The center position with homogenized properties moves to down-side faster than previous model as temperature increase, and snap-through are delayed from equilibrium point due to decreasing stiffness. The bifurcation point present early using MTS, and the symmetric deflection of the model with homogenized properties is restored faster than previous model based on neutral surface. For considering heat transfer effects, the snap-through point is appeared early than previous model as using rule of mixture method, and the bifurcation can be occurred slowly than the previous model regardless of volume fraction with clamped boundary condition. The distributions of plate are differ from each condition, and then homogenized heat conduction affects highly than other effective material properties for thermal post-buckling behavior. In dynamic analysis, as the reference plane is changed, the amplitude of FGMs with simply-supported are increased, and results based on homogeneous scheme are changed according to boundary conditions. As a result, the clamped model are more stable than simply-supported model for both static and dynamic behavior.

References

[1] M. Niino, T. Hirai and R. Watanabe, "The functionally gradient materials", Journal Japan Soc. Composite Materia, vol 13, pp. 257-264.

[2] Y. Miyamoto, W. A. Kaysser, B. H. Rabin, A. Kawasaki and Renee G. Ford, "Functionally Graded Materials: Design, Processing and Applications," Kluwer Academic Publishers, Boston, 1999, pp. 1-6.

[3] M. Bouazza, A. Tounsi, E. A. Adda-Bedia and A. Megueni, "Thermoelastic Stability Analysis of Functionally Graded Plates: An Analytical Approach", Computer Material Science, 2010; 49: 865–870.

[4] M. B. Bouiadjra, M. S. Ahmed Houari and A. Tounsi, "Thermal buckling of functionally graded plates according to a four-variable refined plate theory", Journal of Thermal Stresses, 2012;35: 677–694.

[5] S. R. Li, J. H. Zhang and Y. G. Zhao, "Thermal post-buckling of functionally graded material Timoshenko beams", Applied Mathematics and Mechanics, 2006, vol. 27, pp. 803-810.

[6] T. Prakash, M. K. Singha and M. Ganapathi, "Thermal postbuckling analysis of FGM skew plates", Engineering Structures, 2008, vol30, pp 22-32.

[7] H. S. Shen, "Thermal postbuckling behavior of shear deformable FGM plates with temperature-dependent properties", International Journal of Mechanical Sciences, 2007, vol. 49, pp. 466-478.

[8] S. L. Lee and J. H. Kim, "Thermal post-buckling and limit-cycle oscillation of functionally graded panel with structural damping in supersonic airflow", Composite Structure, 2009, vol.91, pp. 205-211.

[9] C. Y. Lee and J. H. Kim, "Thermal post-buckling and snap-through instabilities of FGM panels in hypersonic flows", Aerospace Science and Technology, 30(2013) 175-182.

[10] Achchhe Lal, K. R. Jagtap and B.N. Singh, "Post buckling response of functionally graded materials plates subjected to mechanical and thermal loadings with random material properties", Applied Mathematical Modeling, 2013 vol.37, pp. 2900-2920.

[11] K. M. Liew, J. Yang and S. Kitipornchai, "Thermal post-buckling of laminated plates comprising functionally graded materials with temperature-dependent properties", Journal of Applied Mechanics, 2004,vol.71, pp. 839-850.

[12] H. M. Navazi and H. Haddapour, "Aero-thermoelastic stability of functionally graded plates", Composite Structure ,2007, vol. 80, pp. 580-587.

[13] K. J. Sohn and J. H. Kim "Structural stability of functionally graded panels subjected to aero-thermal loads", Composite Structures, 2008, vol. 82, pp. 317-325.

[14] T. Prakash and M. Ganapathi, "Supersonic flutter characteristics of functionally graded flat panels including thermal effects", Composite Structures, 2006, vol. 72, pp.10-18.

[15] I. Lee, D.M. Lee and I. K. Oh, "Supersonic flutter analysis of stiffened laminated plates subject to thermal load", Journal of Sound and Vibration, 1999;,vol. 224, pp. 49-67.

[16] H. H. Ibrahim, M. Tawfik and M. Al-Ajmi, "Thermal buckling and nonlinear flutter behavior of functionally graded materials panels", Journal of Aircraft, 2007, vol. 44, pp. 1610-1618.

[17] H. Haddadpour, H. M. Navazi and F. Shadmehri. "Nonlinear oscillation of a fluttering functionally graded plates, Composite Structures, 2007, vol. 72, pp. 242-250.

[18] T. Prakash, M.K. Singha and M. Ganapathi, "Influence of neutral surface position on the nonlinear stability behavior of functionally graded plates", Computer Mechanics, 2008, vol. 43, pp. 341-350.

[19] D.G. Zhang, "Modeling and analysis of FGM rectangular plates based on physical neutral surface and high order shear deformation theory", International Journal of Mechanic Science, 2013, vol. 68, pp. 92–104.

[20] H. Yaghoobi and A. Fereidoon, "Influence of neutral position on deflection of functionally graded beam under uniformly distributed", World Applied Science Journal, 2010, vol. 10, pp.337-341.

[21] T. Mori and K. Tanaka, "average stress in matrix and average elastic energy of materials with mis-fitting inclusions". Acta Metall Mater, 1973, vol. 21, pp. 571-574.

[22] H.S. Shen and Z.X. Wang, "Assessment of Voigt and Mori-Tanaka models for vibration analysis of functionally graded plates", Composite Structures, 2013, vol.47, pp. 90-104.

[23] Y. Kiani and M. R. Eslami, "Thermal post-buckling of imperfect circular FGM plates: examination of Voigt, Mori-tanaka and self-consistent schemes", J Press Vessel Technol (2014), http://dx.doi.org/10.1115/1.4026993.

[24] A. H. Akbarzadeh, A. Abedini and Z. T. Chen, "Effect of micromechnical models on strucutral responses of functionally graded plates", Composite Structure, 2015, vol. 119, pp. 598-609.

[25] J.N. Reddy and C.D. Chin, "Thermo-mechanical analysis of functionally graded cylinders and plates", Journal of Thermal Stresses, 21:6 593-626.

[26] D.G. Zhang and Y.H, Zhou. "A theoretical analysis of FGM thin plates based on physical neutral surface", Computer Material Science, 2008, vol. 44, pp. 716-720.

[27] B.W. Rosen and Z. Hashin, "Effective thermal expansion coefficients and specific heats of composite materials", International Journal of Engineering Science, 1970, vol. 8, pp. 157–173.

[28] H. Hatta and M. Taya, "Effective thermal conductivity of a misoriented short fiber composite", Journal of Applied Physic, 1985, vol. 58, pp.2478–2486.

[29] R. Javaheri and M. R Eslami, "Thermal buckling of functionally graded plates". AIAA Journal , 2002, vol. 40, pp.162–169.

[30] Y. H. Lee, S. I. Bae and J. H. Kim, “Thermal buckling behavior of functionally graded plates based on neutral surface”, Composite Structure, 2016, vol. 137, pp. 208-214.

[31] E. Efraim and M. Eisenberger, "M. Exact vibration analysis of variable thickness annular isotropic and FGM plates". Journal of Sound Vibration, 2007, vol. 299,pp. 720-38.

[32] D. A. R. Mohammad, N. U. Khan and V. Ramamurti, "On the role of Rayleigh damping", Journal of Sound Vibration, 1995, vol. 185, pp. 207-218.

[33] R. D. Cook, D. S. Malkus, M. E. Plesha and R.J. Witt, "Concept and applications of finite element analysis", New York: John Wiley & Sons; 2002.

[34] O. C. Zienkiewicz, R. L. Taylor and J. M. Too, "Reduced integration technique in general analysis of plates and shells", International Journal of Numerical Methods Engineering,1971, vol. 3, pp. 275-290.

[35] P. C. Zhai, C.R. Jiang, Q. J. Zhang, J. B. Holt, M. Koizumi, T. Hirai and Z. A. Munir, editors. "Ceramic Transactions: Functionally Gradient Materials", Westerville: The American Ceramic Society; 1993, pp. 449.

[36] C. Y. Lee and J. H. Kim, "Evaluation of homogenized effective properties for FGM panels in aero-thermal environments", Composite Structures, 2015,vol.120, pp. 442-450.

[37] Y. H. Lee and J. H. Kim, “Estimation of thermal buckling for FGM panels using micro-mechanical properties”, Composite Structure, 2015, Submitted.

[38] S. L. Lee and J. H. Kim, "Thermal post-buckling and the stability boundaries of structurally damped functionally graded panel in supersonic airflows", Composite Structure, 2010, vol.92, pp. 422-429.

Table 1
Material properties of metal and ceramic based on temperature-dependent [25].

Properties		P_{-1}	P_0	P_1	P_2	P_3
Si_3N_4	$E(Pa)$	0	348.43e9	-3.070e-4	2.160e-7	-8.946e-11
	$\alpha(1/K)$	0	5.8723e-6	9.095e-4	0	0
	$k(W/mK)$	0	13.723	-1.032e-3	5.466e-7	-7.876e-11
	ν	0	0.24	0	0	0
$SUS304$	$E(Pa)$	0	201.04e9	3.079e-4	-6.534e-7	0
	$\alpha(1/K)$	0	12.33e-6	8.086e-4	0	0
	$k(W/mK)$	0	15.379	-1.264e-3	2.092e-6	-7.223e-10
	ν	0	0.3262	0	0	0
Al_2O_3	$E(Pa)$	0	349.55e9	-3.853e-4	4.027e-7	-1.673e-10
	$\alpha(1/K)$	0	6.8269e-6	1.838e-4	0	0
	$k(W/mK)$	-1123.6	-14.087	-6.227e-3	0	0
	ν	0	0.31	0	0	0
Ni	$E(Pa)$	0	233.95e9	-2.794e-4	3.998e-9	0
	$\alpha(1/K)$	0	9.9209e-6	8.705e-4	0	0
	$k(W/mK)$	0	187.66	-2.869e-3	4.005e-6	-1.983e-9
	ν	0	0.26	0	0	0

Table 2

Flutter boundaries of FGMs plates with and without structurally damping.

Volume fraction index	Prakash and Ganapathi [6] (without damping)		Lee and Kim [38] (with damping)		Present (with damping)	
	$\left\|\omega_{cr}^{*2}\right\|$	λ_{cr}	$\left\|\omega_{dcr}^{*2}\right\|$	λ_{dcr}	$\left\|\omega_{dcr}^{*2}\right\|$	λ_{dcr}
0	775.78	9661.35	783.2	9672.5	783.2	9672.5
0.5	666.01	4575.07	674.5	4585.4	674.1	4583.7
1	625.78	3515.57	631.2	3522.2	629.7	3519.8
2.5	590.23	2685.94	597.5	2691.1	596.9	2688.5
5	571.48	2348.72	576.6	2353.3	571.1	2350.2

Table 3
Comparison of up and down-side deflection according to reference plane.

Temperature change (ΔT)		16	20	40	60	80
Reference plane						
Mid-plane	Up-side	0.3966	0.6472	1.2875	1.6916	2.0068
	Down-side	-0.6515	-0.8332	-1.3946	-1.7571	-2.0391
	Difference (%)	39.1221	22.3143	7.6843	3.7242	1.5839
Neutral surface	Up-side	-0.6549	0.6109	1.3013	1.7064	2.0204
	down-side		-0.8213	-1.3697	-1.7342	-2.0207
	Difference (%)		25.6116	4.9897	1.6011	0.01189

Table 4
Comparison of up and down-side deflection using homogenized properties

Temperature change (ΔT)		14	20	30	40	50	60
Reference plane							
Rule of mixture	Up-side		0.6109	1.0291	1.30138	1.5197	1.7064
(Neutral surface)	Down-side	-0.5556	-0.8213	-1.1333	-1.3697	-1.5651	-1.7342
	Difference (%)		25.6116	9.1903	4.9897	2.9019	1.6011
Mori-Tanaka	Up-side	0.2998	0.8697	1.2632	1.5476	1.7809	1.9821
(Neutral surface)	Down-side	-0.7472	-1.0145	-1.3398	-1.5912	-1.8011	-1.9834
	Difference (%)	59.8654	14.2702	5.7188	2.7356	1.1145	0.0630

Table 5
Limit cycle amplitudes according to reference plane

Direction	Limit cycle amplitudes (w/h)			
	Boundary Condition			
	Simply-supported		Clamped	
	Mid-plane	Neutral	Mid-plane	Neutral
Up-side	0.0693	0.0717	0.0612	0.0612
Down-side	-0.0709	-0.0707	-0.0572	-0.0573

Table 6
Limit cycle amplitudes using homogenized properties.

Direction	Limit cycle amplitudes (w/h)			
	Boundary Condition			
	Simply-supported		Clamped	
	ROM	MTS	ROM	MTS
Up-side	0.0717	0.0612	0.0612	0.0719
Down-side	-0.0707	-0.0571	-0.0572	-0.0707

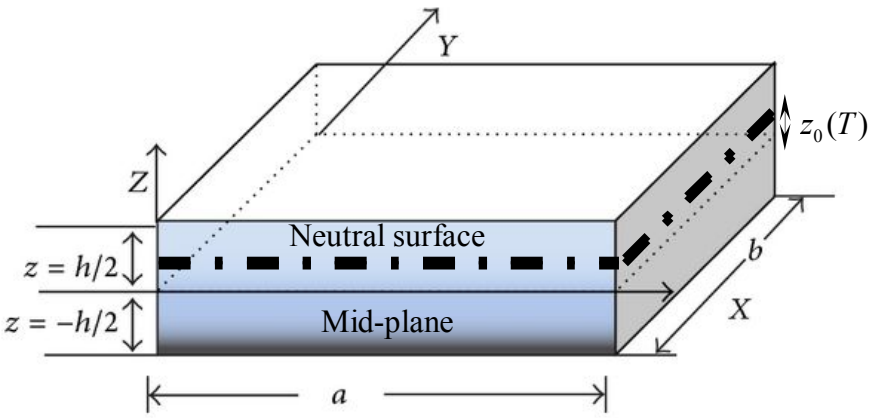

Fig. 1. A FGM plate

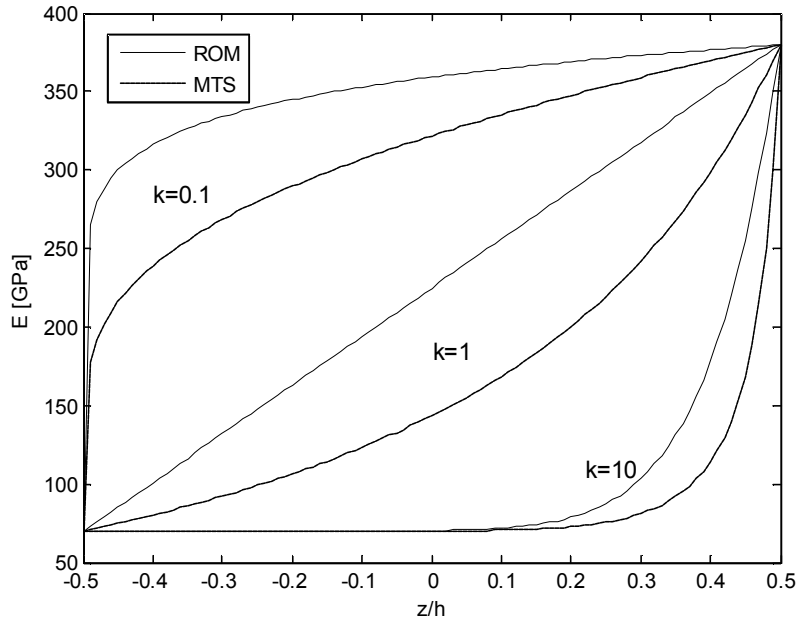

(a)

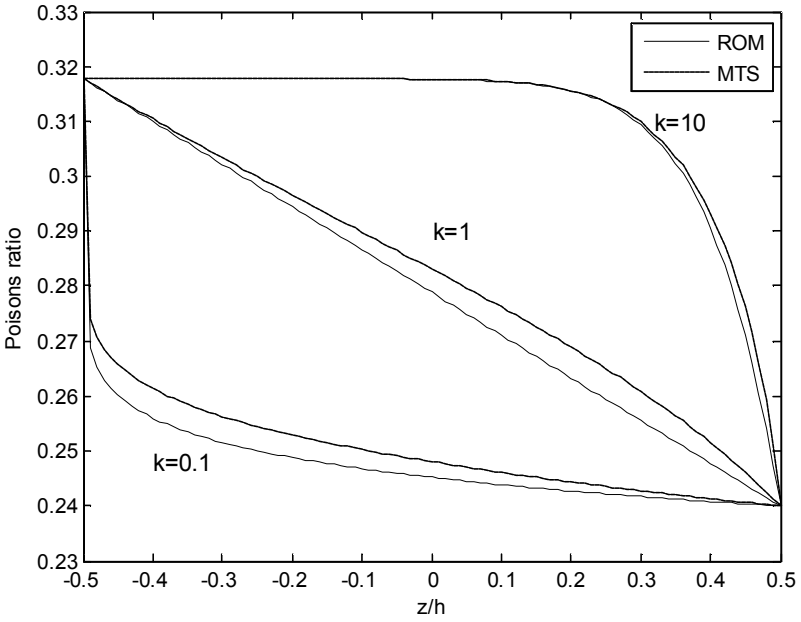

(b)

Fig. 2. Effective materials properties through the thickness distribution. (a) Young's modulus; (b) Poisson's ratio

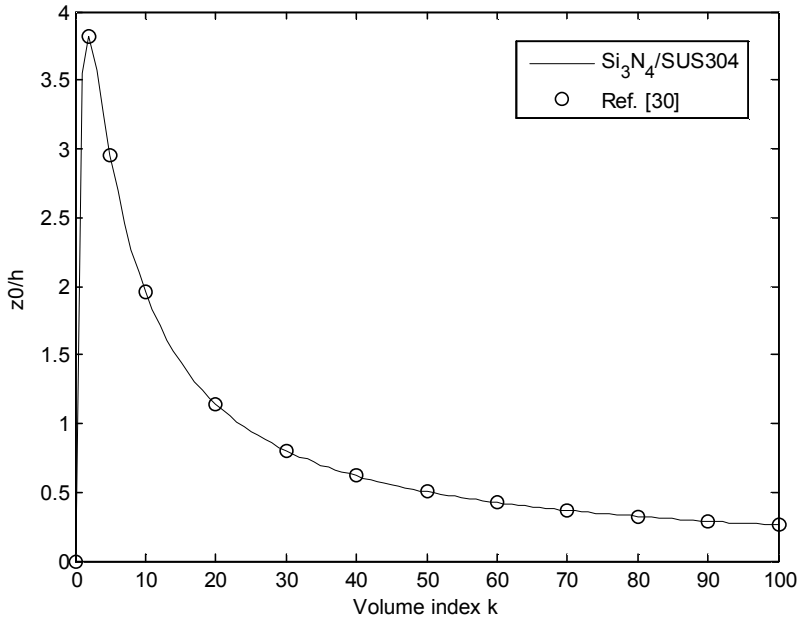

Fig. 3. Non-dimensional neutral surface position from mid-plane.

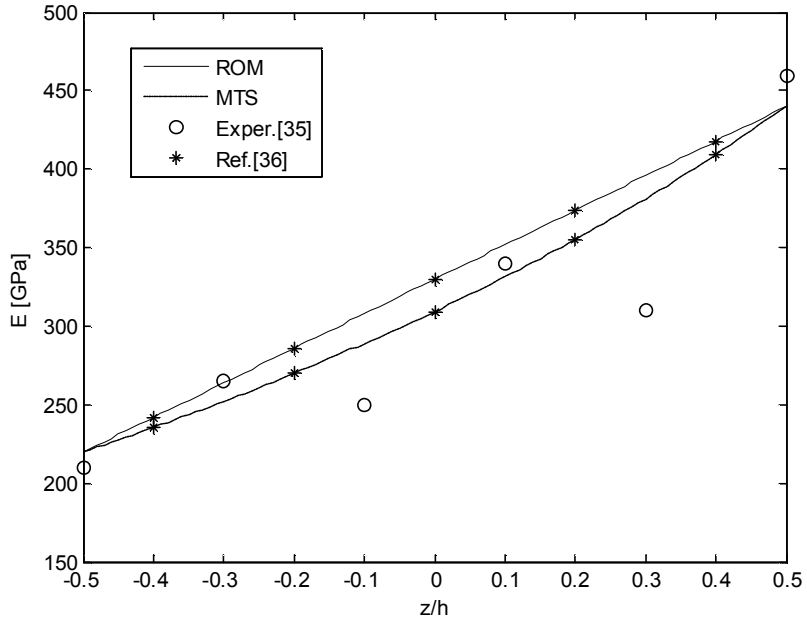

(a)

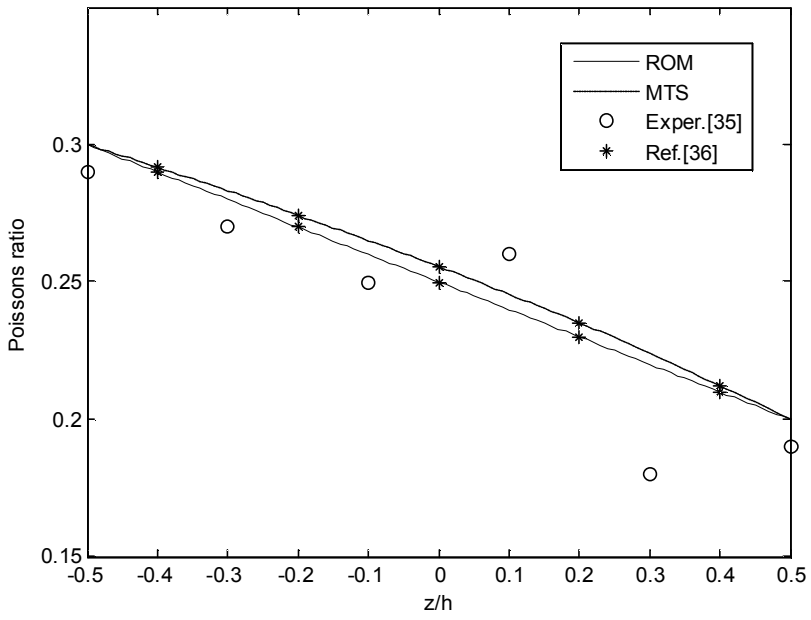

(b)

Fig. 4. Comparison of the effective properties
(a) Variation of Young's modulus ; (b) Variation of Poisson's ratio

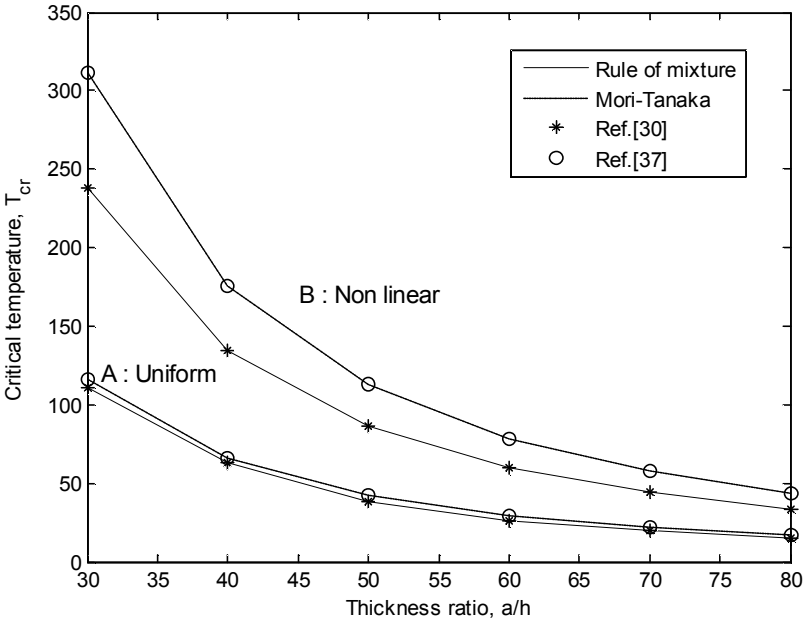

(a)

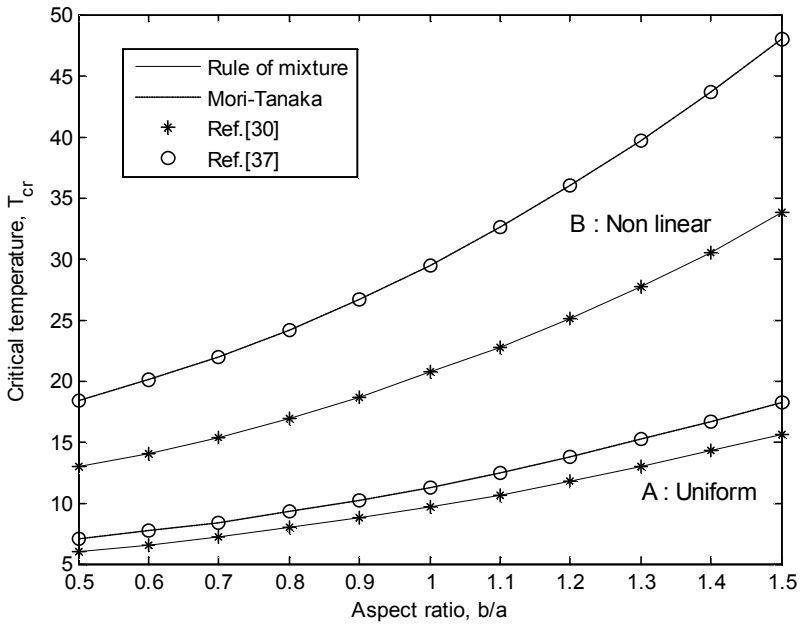

(b)

Fig. 5. Linear buckling temperature based on neutral surface
(a)Thickness; (b) Aspect ratio

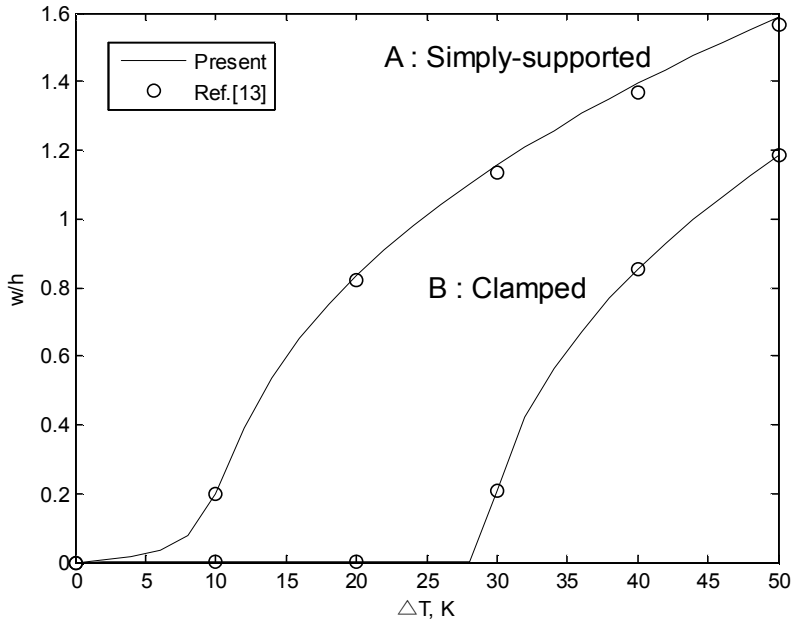

Fig. 6. Non-dimensional center deflection for boundary conditions

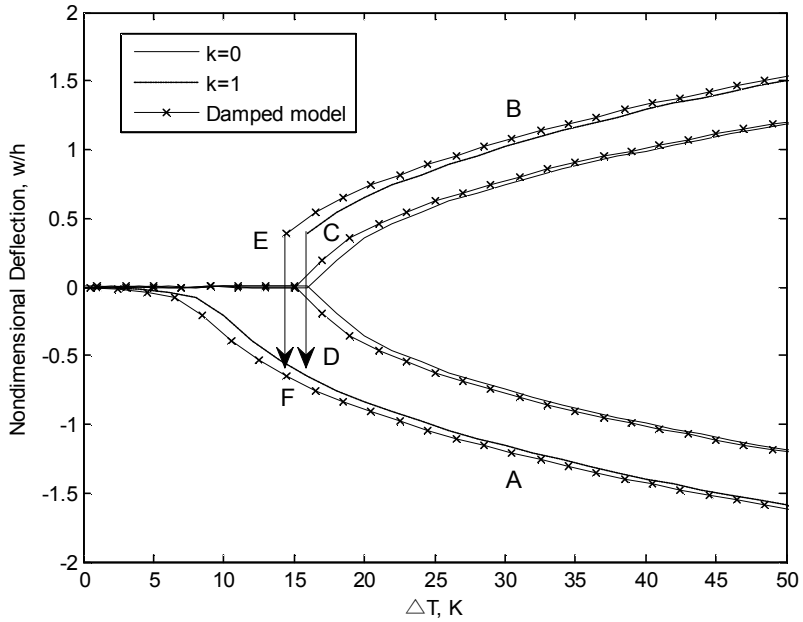

(a)

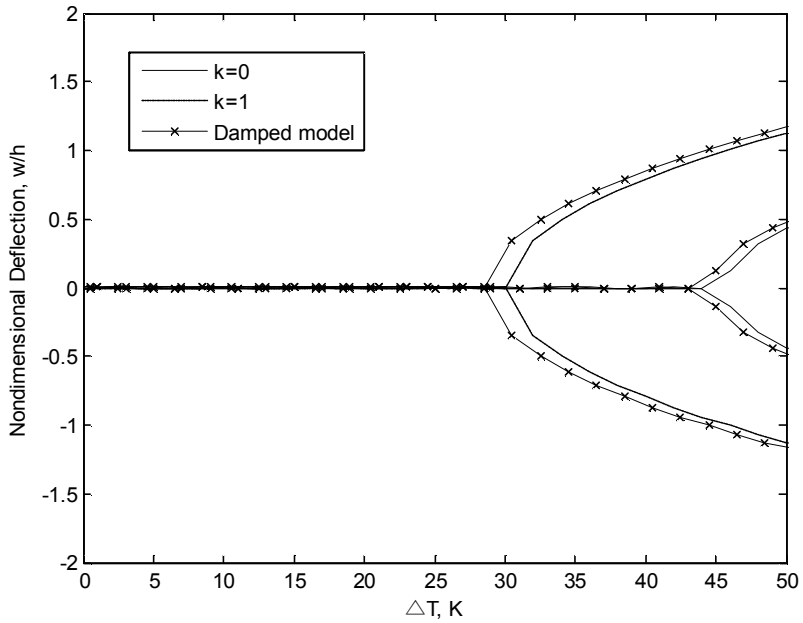

(b)

Fig. 7. Non-dimensional center deflection with and without damping effect without heat conduction ($\Delta T = 300K + \Delta T$)
(a) Simply supported boundary condition ; (b) Clamped

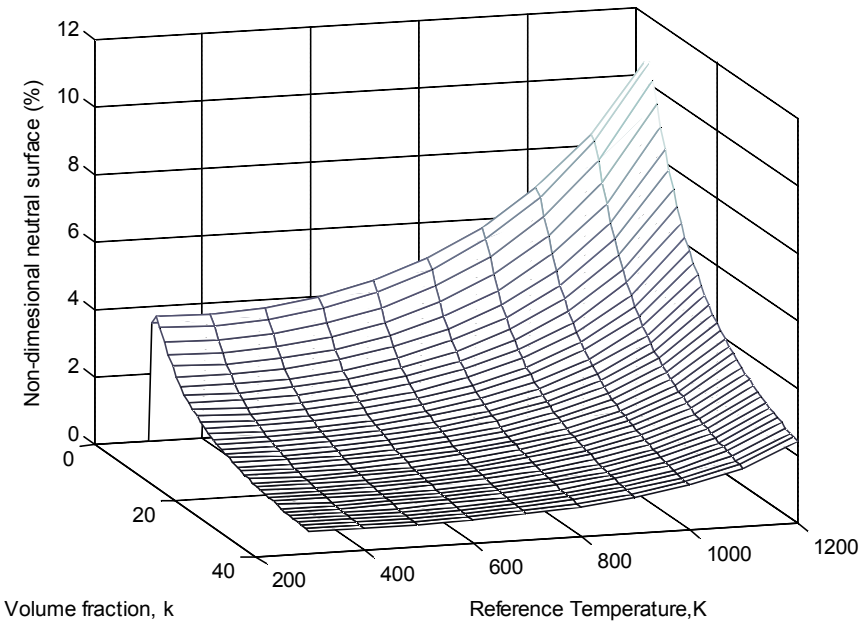

Fig. 8. Neutral surface shift due to volume index and temperatures.

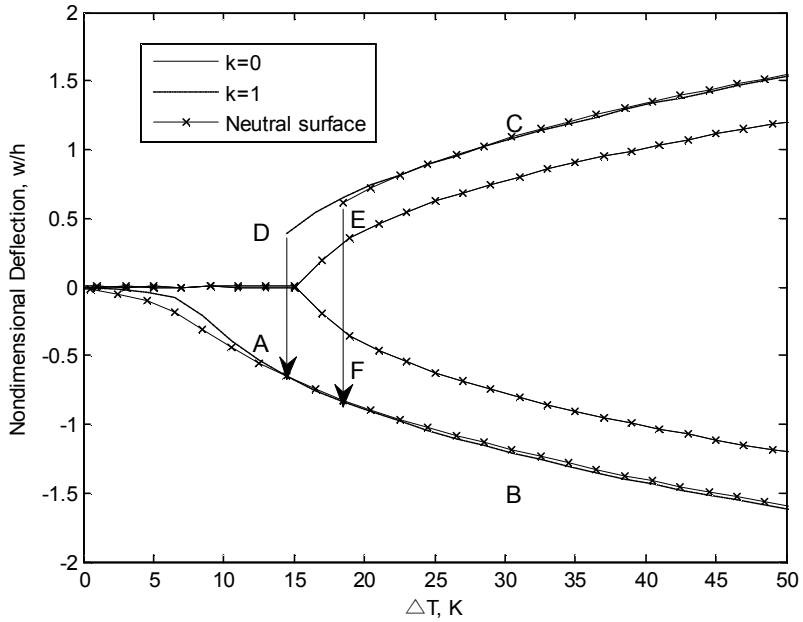

(a)

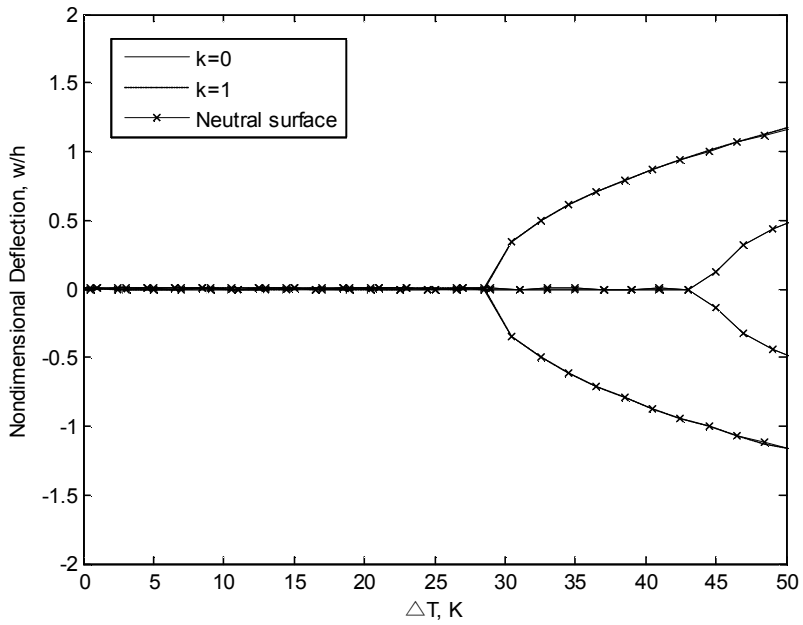

(b)

Fig. 9. Non-dimensional center deflection according to reference plane without heat conduction ($\Delta T = 300K + \Delta T$)
(a) Simply supported boundary condition ; (b) Clamped

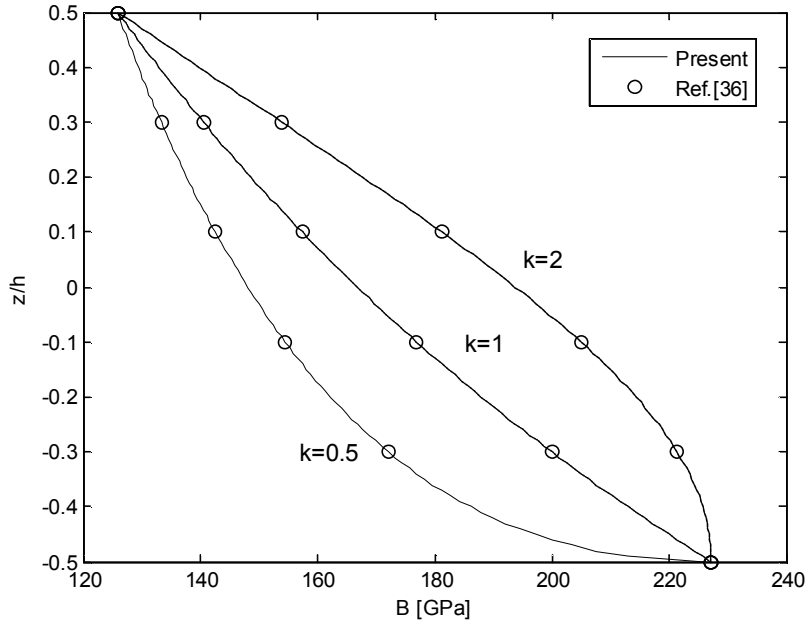

(a)

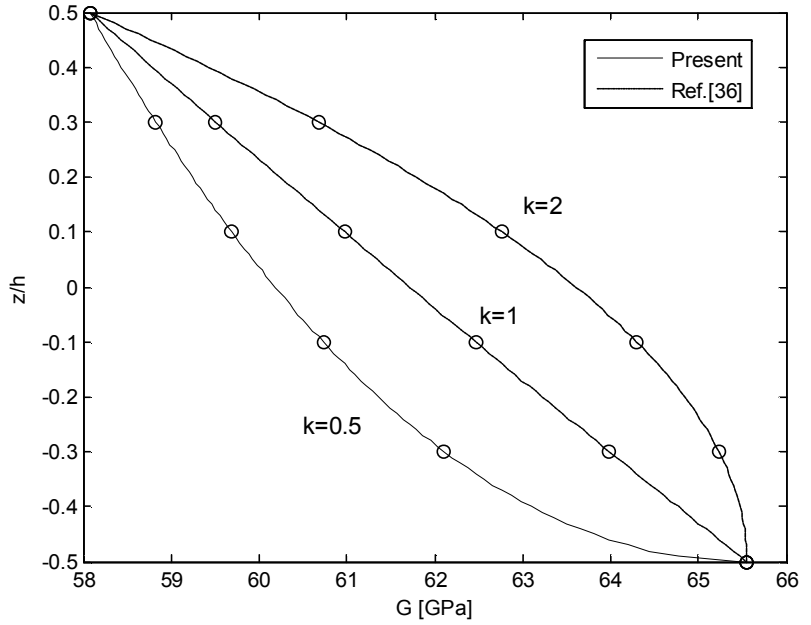

(b)

Fig. 10. Homogenized modulus of FGMs plate
(a) Bulk modulus ; (b) Shear modulus

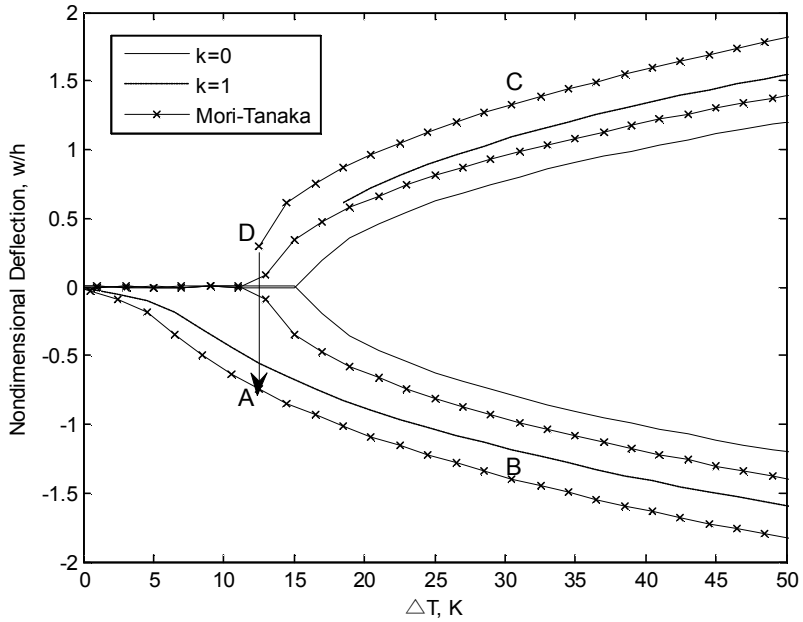

(a)

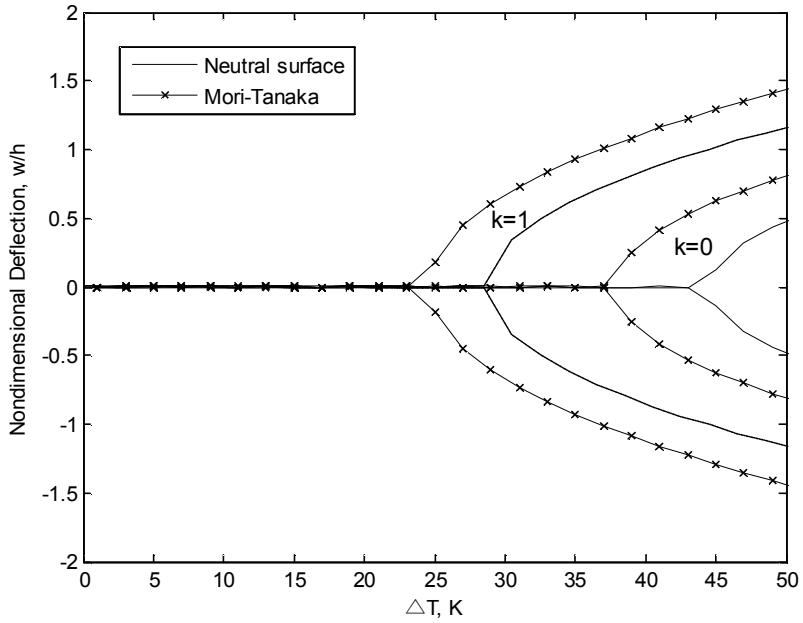

(b)

Fig. 11. Non-dimensional center deflection according to homogenization scheme without heat conduction ($\Delta T = 300K + \Delta T$)
(a) Simply supported boundary condition ; (b) Clamped

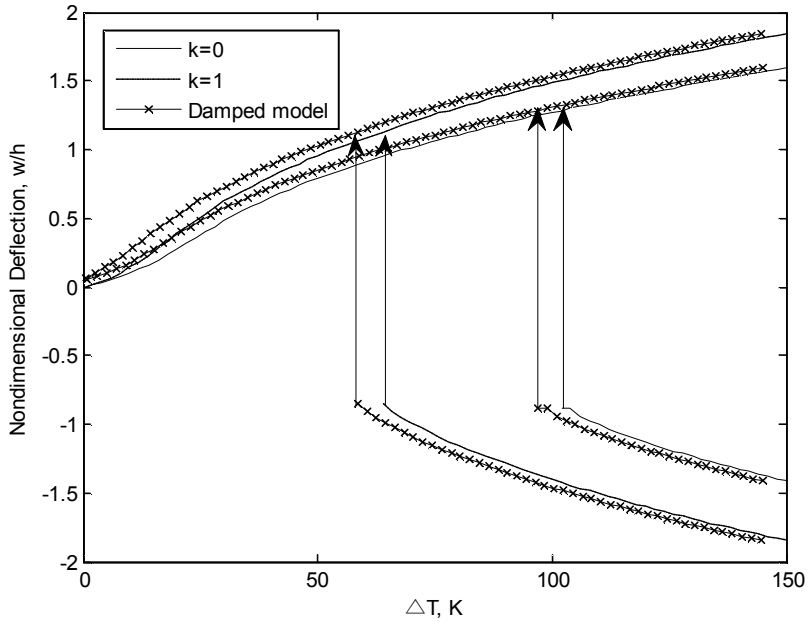

(a)

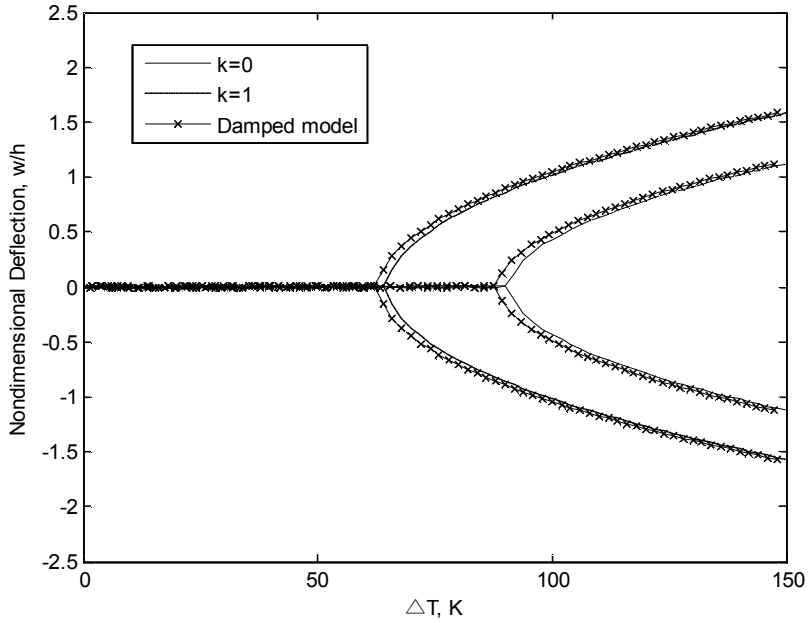

(b)

Fig. 12. Non-dimensional center deflection with and without damping effect considering heat conduction($\Delta T = 300K + \Delta T$)
(a) Simply supported boundary condition ; (b) Clamped

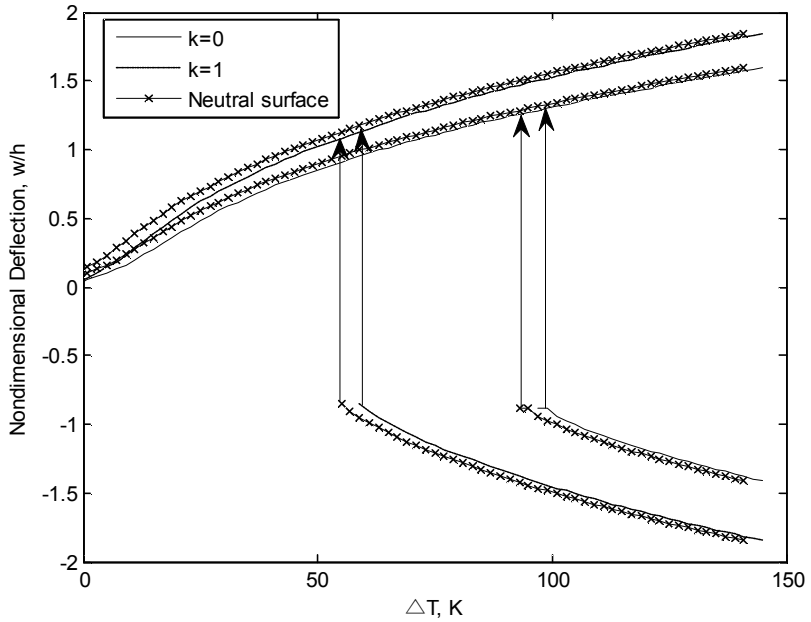

(a)

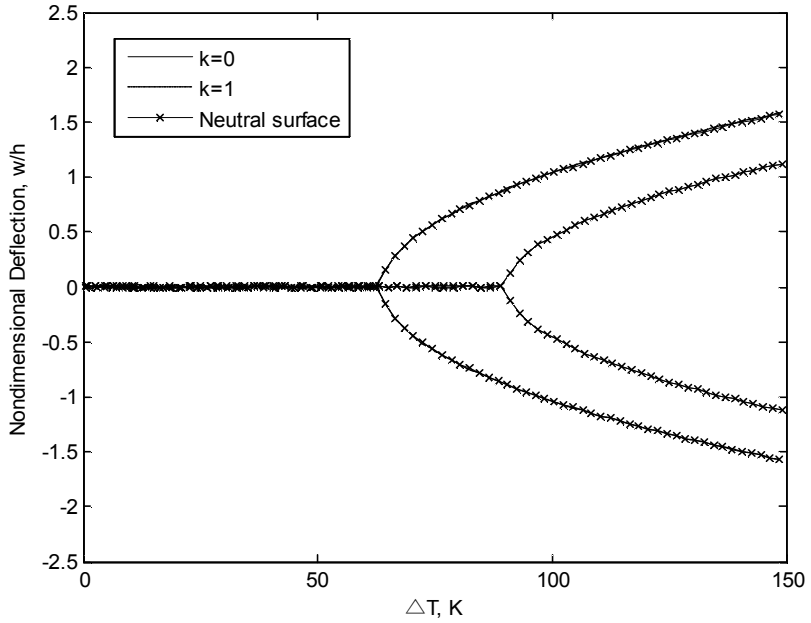

(b)

Fig. 13. Non-dimensional center deflection according to reference plane considering heat conduction($\Delta T = 300K + \Delta T$)
(a) Simply supported boundary condition ; (b) Clamped

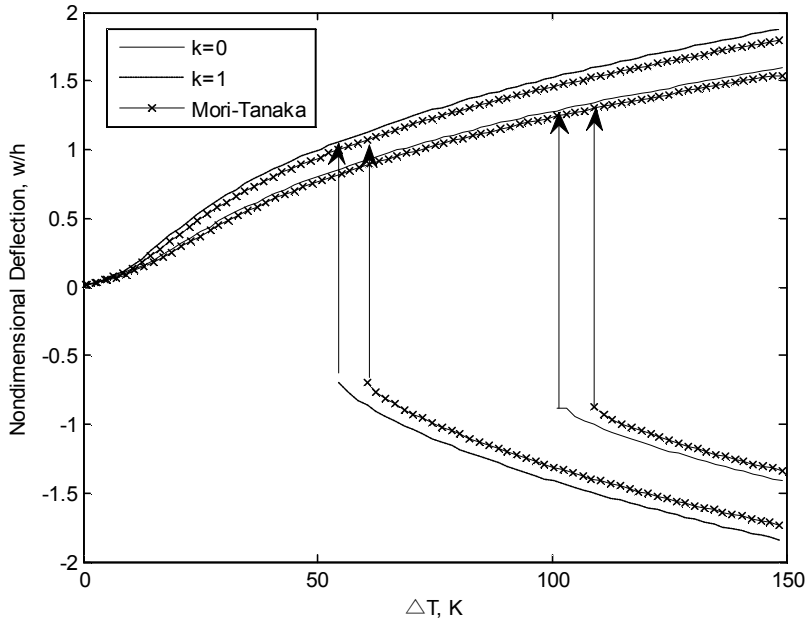

(a)

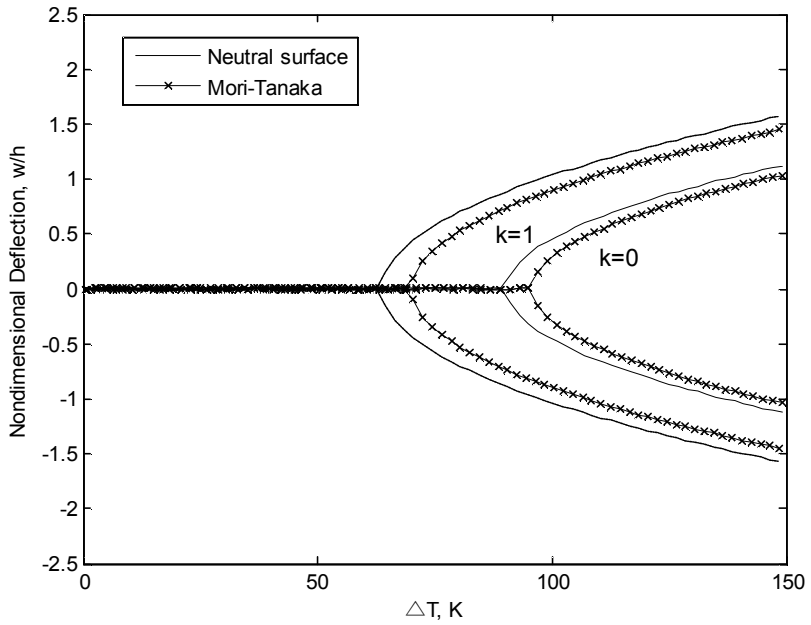

(b)

Fig. 14. Non-dimensional center deflection according to reference plane considering heat conduction ($\Delta T = 300K + \Delta T$)
(a) Simply supported boundary condition ; (b) Clamped

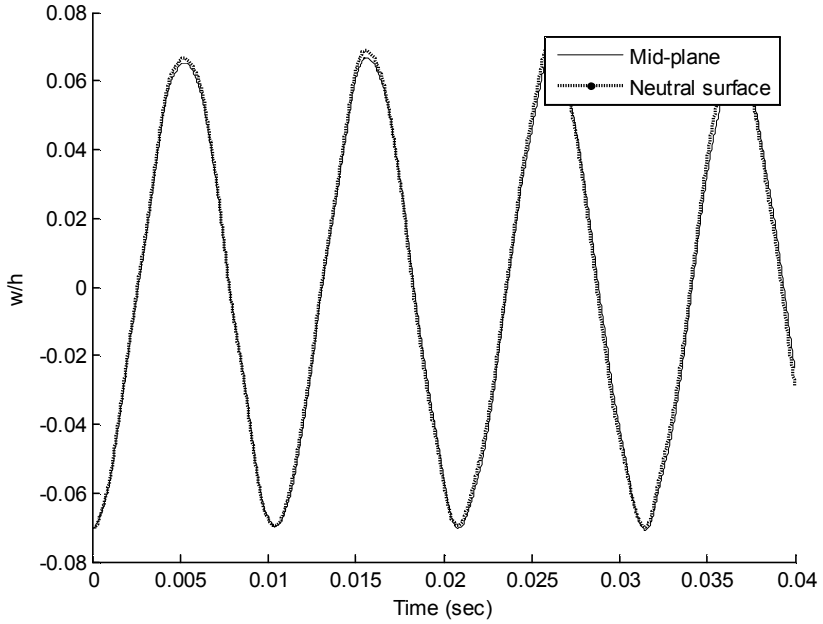

(a)

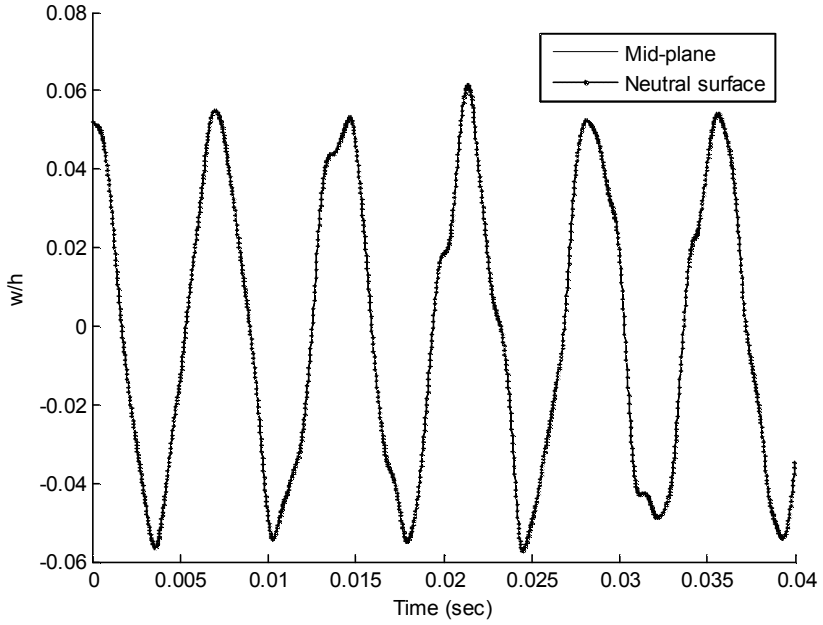

(b)

Fig. 15. LCO of plates according to reference plane without heat transfer effect
(a) Simply supported boundary condition ; (b) Clamped

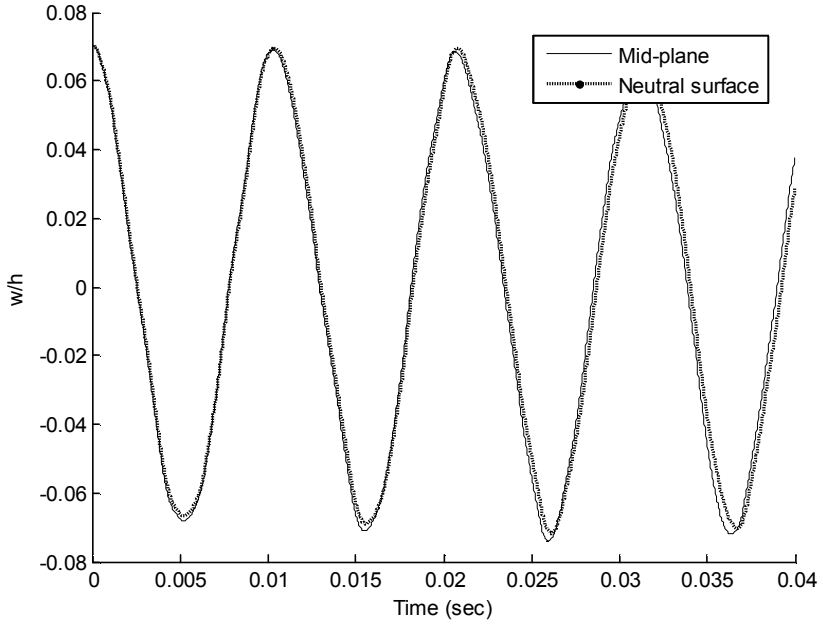

(a)

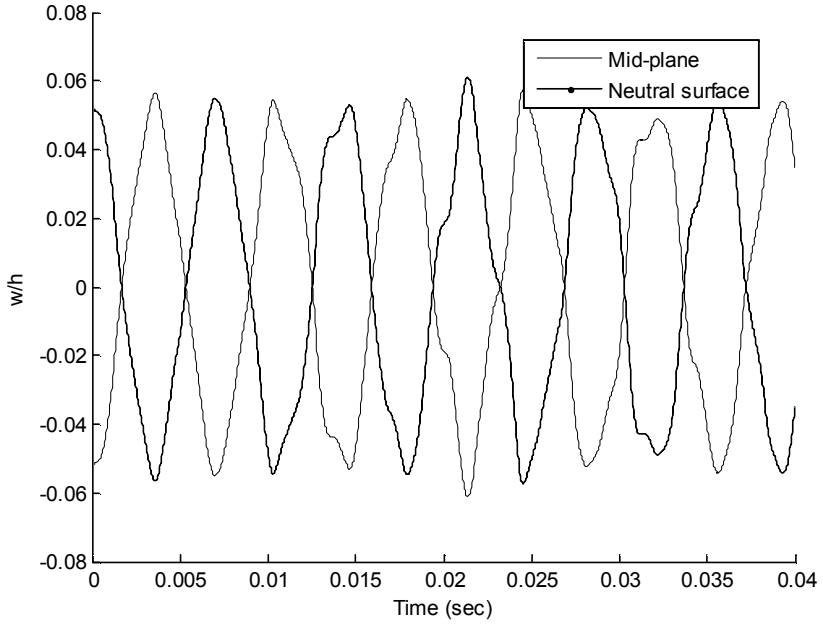

(b)

Fig. 16. LCO of plates according to reference plane with heat transfer effect
(a) Simply supported boundary condition ; (b) Clamped

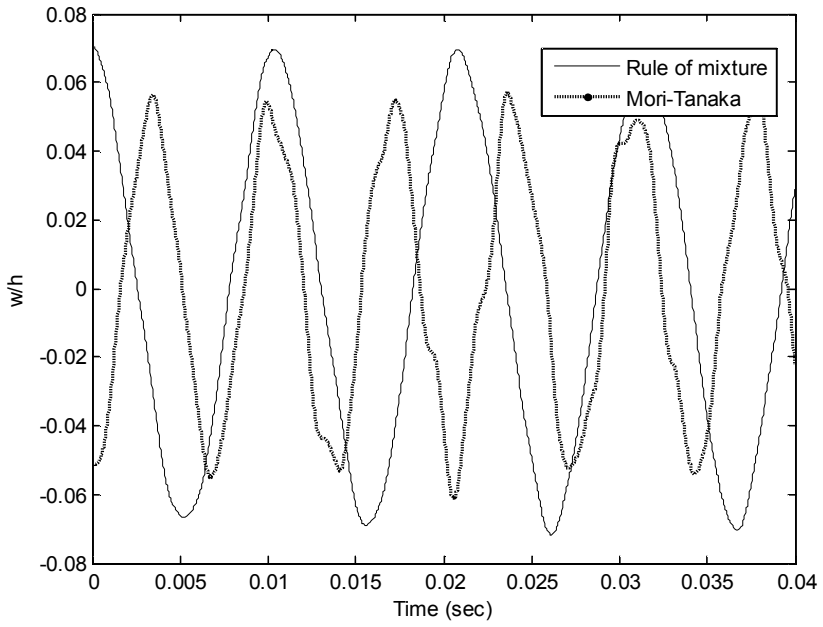

(a)

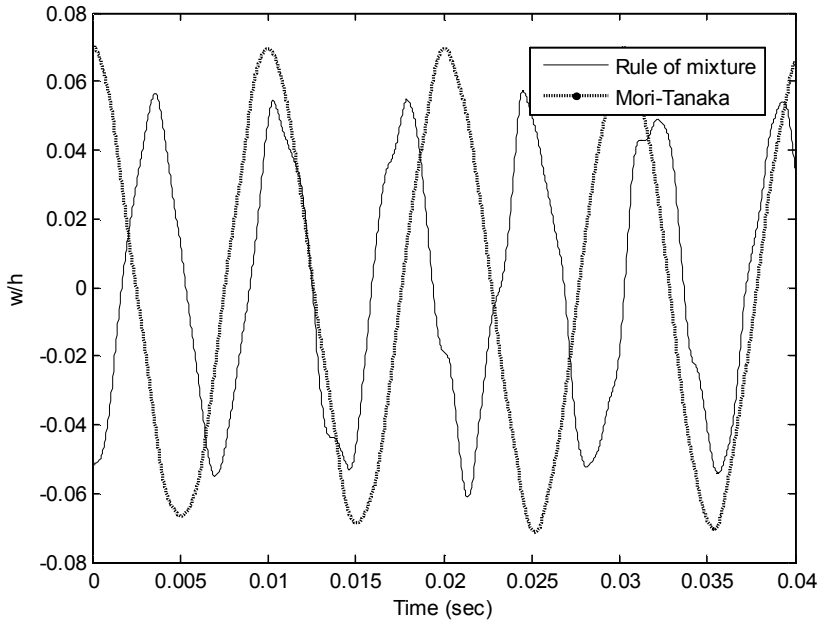

(b)

Fig. 17. LCO of plates using homogenized properties with heat transfer effect
(a) Simply supported boundary condition ; (b) Clamped

국문초록

본 논문에서는 균질화 기법을 사용한 중립면 기초 구조 감쇠된 경사기능 재료의 열적 후좌굴과 제한주기 진동 행동 특성 관하여 연구하였다. 경사기능재료는 금속과 세라믹으로 구성되며 두께방향으로 연속적인 물성치 변화를 갖는다. 경사기능 재료의 두께 방향 비대칭성으로 인해 기존에 사용된 중앙면이 아닌 중립면을 기준면으로 채택하며, 온도의 의존적인 물성치를 사용하기 때문에 중립면도 온도에 따라 변화하게 된다. 또한, 열적 조건에서 경사기능재료의 균질화 모델링을 소개하며, 이 방법은 경사기능재료 해석을 하는데 좀 더 실제적인 방법이 된다. 균질화 기법 중에서도 분자 상호 작용을 고려한 모리-다나카 방법을 채택하였는데, 모리-다나카 방법은 체적, 전단 탄성률을 통하여 균질화된 물성치를 구해낸다.

지배방정식은 1 차 전단이론과 von Karman 변형률-변위 관계를 기초로 구조적 비선형성을 고려하며, 유한요소 해석 방법을 통해 수치 결과를 알아낸다. 이때, Newton-Raphson 방법을 통해 열적 후좌굴을 해석하며, NewMark 의 시간적분법을 통해 제한주기 진동 결과를 알아낸다. 기준면의 변화와 균질화 접근이 경사기능 판의 열적 후좌굴과 플러터 특성에 미치는 영향에 대해 분석하였고, 이를 위해 이전에 연구된 결과들과 비교하였다. 중립면을 기준면으로 채택할 경우, 결과의 큰 차이는 없었지만 평형점이 갑자기 바뀌는 snap-through 현상 이후에 변위 대칭성을 기존 모델보다 더 좋게 가지는 것을 확인하였다. 더욱이, 균질화 기법은 기준면의 효과보다 더 좋은 대칭적 모델을 갖고, 경계조건에 따라 제한주기 진동 경향성에 다른 영향을 주는 것을 확인하였다.

주요어 : 경사기능 재료, 열적 후좌굴, 제한주기 진동, 중립면, 모리-다나카 방법

학 번 : 2014-20679